applied sciences

MDPI

Article

Thermal-Hydraulic-Mechanical Coupling Simulation of CO_2 Enhanced Coalbed Methane Recovery with Regards to Low-Rank but Relatively Shallow Coal Seams

Qianqian Ma [1], Hong Li [1,*], Kun Ji [1,*] and Fengjun Huang [1,2,3]

[1] Faculty of Infrastructure Engineering, Dalian University of Technology, Dalian 116024, China
[2] State Key Laboratory of Geomechanics and Geotechnical Engineering, Institute of Rock and Soil Mechanics, Chinese Academy of Sciences, Wuhan 430071, China
[3] Key Laboratory of Deep Earth Science and Engineering, Sichuan University, Chengdu 610017, China
* Correspondence: hong.li@dlut.edu.cn (H.L.); jk13201@126.com (K.J.)

Abstract: CO_2 injection technology into coal seams to enhance CH_4 recovery (CO_2-ECBM), therefore presenting the dual benefit of greenhouse gas emission reduction and clean fossil energy development. In order to gaze into the features of CO_2 injection's influence on reservoir pressure and permeability, the Thermal-Hydraulic-Mechanical coupling mechanism of CO_2 injection into the coal seam is considered for investigation. The competitive adsorption, diffusion, and seepage flowing of CO_2 and CH_4 as well as the dynamic evolution of fracture porosity of coal seams are considered. Fluid physical parameters are obtained by the fitting equation using MATLAB to call EOS software Refprop. Based on the Canadian CO_2-ECBM project CSEMP, the numerical simulation targeting shallow low-rank coal is carried out, and the finite element method is used in the software COMSOL Multiphysics. Firstly, the direct recovery (CBM) and CO_2-ECBM are compared, and it is confirmed that the injection of CO_2 has a significant improvement effect on methane production. Secondly, the influence of injection pressure and temperature is discussed. Increasing the injection pressure can increase the pressure difference in the reservoir in a short time, so as to improve the CH_4 production and CO_2 storage. However, the increase in gas injection pressure will also lead to the rapid attenuation of near-well reservoir permeability, resulting in the weakening of injection capacity. Also, when the injection temperature increases, the CO_2 concentration is relatively reduced, and the replacement effect on CH_4 is weakened, resulting in a slight decrease in CBM production and CO_2 storage.

Keywords: CO_2 sequestration; enhanced coalbed methane recovery; permeability; Thermal-Hydraulic-Mechanical coupling

check for updates

Citation: Ma, Q.; Li, H.; Ji, K.; Huang, F. Thermal-Hydraulic-Mechanical Coupling Simulation of CO_2 Enhanced Coalbed Methane Recovery with Regards to Low-Rank but Relatively Shallow Coal Seams. *Appl. Sci.* **2023**, *13*, 2592. https://doi.org/10.3390/app13042592

Academic Editor: Nikolaos Koukouzas

Received: 15 January 2023
Revised: 13 February 2023
Accepted: 14 February 2023
Published: 17 February 2023

Copyright: © 2023 by the authors. Licensee MDPI, Basel, Switzerland. This article is an open access article distributed under the terms and conditions of the Creative Commons Attribution (CC BY) license (https://creativecommons.org/licenses/by/4.0/).

1. Introduction

Since the industrial revolution, human activity has resulted in upraising the concentrations of greenhouse gases, causing an anthropogenic influence on global warming and climate change. If no reduction measures are taken, the global atmospheric temperature will rise by more than 1.5 °C and 2 °C by 2030 and 2050, respectively, according to the global average annual rate of anthropogenic CO_2 emissions from 2011 to 2020 (38.9 billion tons CO_2/year) [1]. Environmental repercussions of global climate change brought on by rising human-caused emissions of heat-trapping greenhouse gases are already ubiquitous, such as accelerated sea level rise, sea ice loss, melting glaciers and ice sheets, more intense heat waves, and plant and animal geographic ranges shifts. Human-caused global climate change is irreversible and will worsen in the coming decades [2]. There is almost a universal agreement that the world cannot sit back and wait for definitive answers on this issue, and that preventive and mitigating measures must be implemented concurrently. CO_2 is recognized as by far the most significant greenhouse gas due to its relative abundance when compared to the other greenhouse gases, accounting for around 64% of the heightened

"greenhouse effect". Therefore, reducing CO_2 emissions to the atmosphere is a significant challenge in mitigating anthropogenic effects on climate change.

Currently, heavy energy-consuming sectors are moving to developing nations [3], which results in the rising phase of CO_2 emissions in developing countries. The CO_2 emission reduction at the expense of reducing the amount of industrial activity harms economic development, generating two competing demands to keep both economic growth and substantial CO_2 emission reduction for developing countries, especially for China, the major developing country in the world [4]. Carbon Capture, Utilization and Storage (CCUS), as one pathway to carbon neutrality goals, can meet these two competing needs. Nowadays, more than 100 countries have proposed corresponding carbon neutrality programs. According to the prediction of existing research, fossil energy will still play an important role by 2050, and Carbon Capture, Utilization, and Storage (CCUS) is the only technical choice to achieve large-scale zero-emission utilization of fossil energy [5].

CO_2 enhanced coalbed methane recovery (CO_2-ECBM) is an important technical approach of CCUS, which has the dual benefits of greenhouse gas emission reduction and clean fossil energy recovery [6]. Within the coal matrix, the adsorption capacity of CO_2 is higher than that of CH_4 so that CO_2 can replace most of the originally adsorbed CH_4. Thus, the latter is desorbed and swept out. Simultaneously, along the run-through cleats and cracks in coal, CO_2 injection can maintain reservoir energy by improved pressure gradient so that the partial pressure of CH_4 is relatively compensated. CO_2 storage mechanism and storage capacity, and the effect of increasing production of CH_4 are the key technical problems of CO_2-ECBM [7].

At present, CO_2-ECBM technology is not very mature, and it is still in the pilot test or experimental mining stage in the world, and has not achieved large-scale commercial mining appraisal. Table 1 illustrates the existing CO_2-ECBM field experiments and their details. It can be seen from Table 1 that the permeability of coal seams in the United States, Canada and other countries are better, which is one to two orders of magnitude higher than that of Chinese coal. In addition, due to the good adsorption of high-rank coal, most of the experiments are based on middle and high-rank coal seams, and there are few experiments on shallow low-rank coal. Among them, the CSEMP (CO_2 Storage and Enhanced Methane Production) project on which this study is based may be a relatively rare shallow low-rank coal CO_2 injection test project. From the Langmuir adsorption curve, we have known that the CO_2 adsorption capacity of low-rank coal is very small when the pressure is low, and when the pressure increases, the adsorption capacity increases slowly, but the adsorption capacity of high-rank coal is very large when the pressure is low, and the adsorption capacity increases greatly with the increase of pressure. However, it is worth mentioning that the CO_2/CH_4 adsorption ratio of low-rank coal is much larger than that of high-rank coal, which highlights the superiority of CO_2 replacement of CH_4 in low-rank coal.

The gas migration in the CO_2-ECBM process is a very complex process, including the competitive adsorption, diffusion, seepage, coal deformation and temperature exchange of coalbed methane and injected CO_2 gas. Based on the laboratory scale, previous scholars have carried out many studies on the adsorption characteristics of CO_2 and CH_4, the mechanism of gas flow in coal as well as the replacement efficiency and utilization rate of CO_2 by coal. Barbara Dutka [8] carried out an experimental research into the sorption properties of coal briquettes under the various states of stress, proved that the existence of a relation between the stress state, sorption capacity and volumetric deformation of coal. Sun et al. [9] carried out an experimental study on the displacement of methane by CO_2 using eight bituminous and anthracite coals, to evaluate the displacement efficiency and utilization ratio of CO_2. Zheng et al. [10] explored the characterizations of methane desorption and CO_2 displacement under different CO_2 injection pressures or different experimental temperatures using the self-designed NMR-based CO_2 displace methane equipment. Xu et al. [11] proposed a new multi-scale dynamic diffusion-percolation model to compare the old and new model analysis, as well as carefully studying the mechanism of gas flow in coal. Chen et al. [12] studied the the influence of coal water content and gas

injection pressure on CH_4 replacement rate and CO_2 injection ratio based on the adsorption characteristics of coal seam gas injection.

Table 1. Existing CO_2-ECBM field experiments.

Country	Project	Burial Depth (m)	Coal Rank	Permeability (md)	Reference
U.S.A	Allison Unit, San Juan Basin	945	Bituminous coal	30–150	
	Pump Canyon, San Juan Basin	918	Bituminous coal	146–550	[13]
	Tanquary Farms test site, lllinois Basin	274	Bituminous coal	2–7.0	[14]
	Virginia Central Appalachian Basin Coal Test	427–671	Bituminous coal	5–20	[15]
	Lignite Field Validation Test, Williston Basin	335	Lignite	1	[16]
	Black Warrior Basin Coal Test	548 437 237	Bituminous coal	0.1–0.2 10–16	[17]
	Marshall County project, Northern Appalachian Basin	400–530	Bituminous coal	1	[18]
	Buchanan County, Central Appalachian Basin	274–671	Bituminous coal	5–27	
Canada	FBV 4A Micro-Pilot Test, Western Canada Sedimentary Basin		Bituminous coal	3.65	[19]
	ARC ECBM				
	CSEMP	420	Sub-Bituminous coal		
Poland	RECOPOL, upper Silesian coalbasin, Poland	1012–1076	Bituminous coal	0.4–1.5	[20]
Japan	Yubari field test, Ishikari Coal Basin, Japan	890	Bituminous coal	1	[21]
China	Qinshui Basin ECBM 2004	472	Anthracite	12.0/0.95	[22]
	Qinshui Basin ECBM 2010	923	Anthracite	0.002–0.8	[23]
	APP ECBM, Ordos Basin	560	Bituminous coal	0.64	[24]
	Qinshui Basin multiple wells	972	Anthracite	0.002–0.8	

In addition to conducting physical experiments, many scholars have conducted in-depth research on CO_2-ECBM using numerical simulation. V. Vishal et al. [25] carried out research work to understand the technical feasibility of CO_2 driven enhanced CBM recovery in Indian coals using a commercial reservoir simulator, COMET. Hema J. Siriwardane et al. [26] performed a historical fit to the Pump Canyon ECBM field test in the United States using PSU-COALCOMP, where the anisotropy of the reservoir was considered in the model, and the study showed that a more accurate set of parameters could be determined using numerical simulations. The gas migration in the CO_2-ECBM is a process of multi-phase fluid and multi-physical field coupling.

In recent years, scholars have also done some work on CO_2-ECBM multi-physics coupling. The effect of the numerical case is different based on the difference in coal reservoir structure and physical properties. Wu et al. [27] established a gas-solid coupling model to study the migration of binary gases in coal reservoirs, and clarified the distribution of coalbed methane concentration in CO_2-ECBM, but did not consider gas diffusion and competitive adsorption of binary gases. Wang et al. [28] carried out large-scale laboratory tests and deduced the seepage diffusion control equation, but did not consider the deformation of coal. Fang et al. [29,30] established the coupling equations of the diffusion–adsorption–seepage–heat transfer fields of gas. The displacement processes under different pressures and temperatures are simulated by COMSOL. Subsequently, the stress field model and seepage field model were derived, and the numerical simulation of permeability evolution was carried out in COMSOL software. Hemant Kumar et al. [31] established a coupled finite element (FE) model of binary gas flow, diffusion, competitive sorption and permeability change to explore the effect of CO_2 injection on net recovery, permeability evolution and injectivity in uniform and homogeneously permeable reservoir. Wang et al. [32] built a dual porosity/permeability model through accurately expressing the volumetric strain of matrix and fracture which aims to reveal the reservoir permeability evolution during the process of CO_2-enhanced coalbed methane (CO_2-ECBM) recovery. Bai et al. [33] established a fluid-solid coupling model considering gas-water phases and

Klinkenberg effect of CO_2 injection into coal seam for enhancement of gas drainage, parameters of gas pressure, gas content and gas extraction rate after coal seam CO_2 injection were analyzed by using COMSOL software and applied in engineering test. Erlei Su et al. [34] established an improved fully coupled gas migration model for CBM extraction. The permeability rebound and recovery times as well as rebound values are proposed to accurately quantify permeability evolution during CBM extraction. Also, the evolution of coal seam permeability under different CO_2 injection method is discussed. Most of the above scholars only consider a single or several physical fields in their research. In addition, many scholars [29,32,35] have studied the Thermal-Hydraulic-Mechanical coupling of CO_2-ECBM, but most of these studies are based on deep unminable coal seams. At present, there are few numerical simulation studies on the Thermal-Hydraulic-Mechanical multi-physical coupling of shallow low-rank coal. The buried depth of the deep unminable coal seam is large. Under geological conditions of high temperature and high pressure, CO_2 is likely to exist in the supercritical state, so the change in its physical parameters may not be obvious. Therefore, previous studies regard fluid physical parameters as constants,which is barely acceptable. However, in the temperature and pressure range of shallow low-rank coal, the physical parameters of CO_2 are prone to mutation. Therefore, it is very inadvisable to regard the physical parameters as constants.

This study is based on the Canadian CSEMP shallow low-rank coal project to carry out CO_2-ECBM numerical simulation research. The porosity-permeability evolution model is substituted into the fluid migration equation, combined with the reservoir deformation equation, the energy conservation equations and the fluid physical parameter evolution equation. Then, a set of coupled partial differential equations is derived. The COMSOL Multiphysics simulation software is used to solve the finite element method. Firstly, this study compared CBM (directly mining) with CO_2-ECBM, affirms the advantages of CO_2-ECBM. The evolution of reservoir pressure, permeability and adsorbed gas content in CO_2-ECBM and CBM engineering are analyzed. Subsequently, the effects of different injection pressures and temperatures on CO_2-ECBM were analyzed. The study has certain guiding significance for the preliminary design of the follow-up CO_2-ECBM project based on shallow low-rank coal.

2. Theory of Modelling

2.1. Fundamental Assumption

The CO_2-ECBM process in CH_4-bearing coal is the fully coupled process of the Thermal-Hydraulic-Mechanical fields, which involves the competitive adsorption of CH_4 and CO_2, the deformation of the coal reservoir, and the heat exchange of the gas and coal skeleton. The following assumptions are required for establishing these fully coupled models: (1) Coal is a homogeneous isotropic body; (2) CH_4 is saturated in the reservoir; (3) The seepage and diffusion of CH_4 and CO_2 conform to Darcy's law and Fick's law, respectively; (4) The deformation of the coal reservoir is infinitesimal deformation.

2.2. Governing Model of the Hydraulic Field

The mass conservation equation of CO_2 and CH_4 gas seepage and diffusion in coal seam is [36]:

$$\frac{\partial m_g}{\partial t} + \nabla \cdot (\rho_i q) + \nabla \cdot (q_d) = 0 \quad (1)$$

where, m_g is the gas mass in per unit volume of coal, kg/m^3; ρ_i is the gas density, kg/m^3; q is seepage velocity, m/s; i = 1, CH_4, i = 2, CO_2.

The seepage of gas in coal seams obeys Darcy's law:

$$q = -\frac{k}{\mu_i} \nabla P_i \quad (2)$$

Gas diffusion in coal seams obeys Fick's first law:

$$q_d = -D_i \cdot \nabla c_i \tag{3}$$

Thus, the following can be obtained:

$$\frac{\partial m_g}{\partial t} - \nabla \cdot \left(\frac{k}{\mu_i} \nabla P_i \cdot \rho_i \right) - \nabla \cdot (D_i \nabla c_i) = Q_i \tag{4}$$

where, D_i is the diffusion coefficient, m^2/s; c_i is the diffusion mass concentration of gas, kg/m^3; Gas mass per unit volume of coal consists of free gas and adsorbed gas [37]:

$$m_g = m_f + m_s = \varphi \rho_i + \rho_c \rho_i \frac{a_i b_i P_i}{1 + b_1 P_1 + b_2 P_2} \tag{5}$$

where, ρ_c is the density of coal, kg/m^3; b_i is the Langmuir adsorption constant of gas, MPa^{-1}; a_i is the langmuir volume constant of gas, m^3/kg.

Thus, available:

$$\frac{\partial \left(\varphi \rho_i + \rho_c \rho_i \frac{a_i b_i P_i}{1 + b_1 P_1 + b_2 P_2} \right)}{\partial t} - \nabla \cdot \left(\frac{k}{\mu_i} \nabla P_i \cdot \rho_i \right) - \nabla \cdot \left(D_i \nabla \frac{\rho_i}{M_i} \right) = Q_i \tag{6}$$

where, k is permeability, m^2; μ_i is the dynamic viscosity coefficient of gas, Pa·s; φ is porosity, zero dimension;

2.3. Governing Model of the Mechanical Field

The deformation of coal is formed under the joint actions of ground stress, gas pressure, gas adsorption/desorption and thermal stress, and the constitutive equation of the mechanical field can be deduced based on the elastic theory of porous media, which is as follows [38]:

$$\varepsilon_{ij} = \frac{1}{2G} \sigma_{ij} - \left(\frac{1}{6G} - \frac{1}{9K} \right) \sigma_{hh} \delta_{ij} - \frac{\alpha}{3K} (P_1 - P_2) \delta_{ij} + \frac{\varepsilon_s}{3} \delta_{ij} + \frac{\alpha_s \Delta T}{3} \delta_{ij} \tag{7}$$

where, ε_{ij} is the strain tensor component, m; G is the shear modulus, MPa; σ_{ij} is a component of the stress tensor; σ_{hh} is the normal stress component; δ_{ij} is Kronecker symbol; α is Biot's coefficient.

Equation (7) is the equilibrium equation characterizing the spatial equilibrium state of coal reservoir, and the strain component and displacement component satisfy Equation (8) [39]

$$\begin{aligned} \sigma_{ij,j} + F_i &= 0 \\ \sigma_{ij} &= \frac{1}{2}(u_{ij} + u_{ji}) \end{aligned} \tag{8}$$

Based on the above equations, the Navier-Stokes equations which can characterize the stress field of coal reservoir can be derived:

$$G u_{i,jj} + \frac{G}{1 - 2v} u_{j,ji} + \alpha P_{1,i} + \alpha P_{2,i} - K \varepsilon_{s,i} + F_i = 0 \tag{9}$$

where, v, Poisson ratio; K_s is the bulk modulus of coal matrix, MPa; K is the bulk modulus of coal, MPa; ε_s is volume strain caused by gas adsorption desorption, $\varepsilon_s = \frac{a_1 b_1 P_1 + a_2 b_2 P_2}{1 + b_1 P_1 + b_2 P_2}$.

2.4. Governing Model of the Thermal Field

According to the law of conservation of energy and Fourier's law, the energy conservation equations of skeleton and gas can be obtained [40].

$$\frac{\partial}{\partial t}\left(\left(\rho C_p\right)_{eff}\right) + \eta_{eff}\nabla T - \nabla\cdot\left(\lambda_{eff}\nabla T\right) + K\alpha_T T\frac{\partial \varepsilon_s}{\partial t} + \sum_{i=1}^{2} q_{sti}\frac{\rho_s\rho_{si}}{M_i}\frac{\partial \varepsilon_v}{\partial t} = 0 \tag{10}$$

where, $(\rho C_p)_{eff}$, is the effective heat capacity, J/m^3·K, η_{eff}, is the effective convective heat transfer coefficient, J/m^2·s, λ_{eff}, is the effective thermal conductivity, W/(m·K):

$$\left(\rho C_p\right)_{\text{eff}} = (1-\varphi)\rho_s C_s + \varphi\left(\frac{M_1 P_1}{RT}C_{g1} + \frac{M_2 P_2}{RT}C_{g2}\right) \tag{11}$$

$$\eta_{\text{eff}} = -\frac{k}{\mu_1}\nabla P_1\rho_{g1}C_{g1} - \frac{k}{\mu_2}\nabla P_2\rho_{g2}C_{g2} \tag{12}$$

$$\lambda_{\text{eff}} = (1-\varphi)\lambda_s + \varphi\left(\lambda_{g1} + \lambda_{g2}\right) \tag{13}$$

where, C_{g1}, C_{g2} is the specific heat capacity of CH_4, CO_2, J/kg·K; λ_{g1}, λ_{g2} is the thermal conductivity of CH_4 and CO_2, W/(m·K).

2.5. Permeability Evolution Equation

Based on gas pressure, temperature and volume change caused by adsorption and desorption of coal matrix, porosity evolution formula can be derived [41,42]:

$$\varphi = \frac{V_p}{V} = 1 - \frac{1-\varphi_0}{1+\varepsilon_v}\left(1 + \frac{\Delta V_s}{V_{s0}}\right) \tag{14}$$

where, V_p is the pore volume of coal, m^3; V is the total volume of coal, m^3; φ_0 is the initial porosity of coal seam; δV_s is the volume change of coal skeleton, m^3; V_{s0} is the initial skeleton volume of coal body, m^3

$$\frac{\Delta V_s}{V_{s0}} = -\frac{\alpha}{K_s}(\Delta P_1 + \Delta P_2) + \Delta\varepsilon_s + \alpha_s\Delta T \tag{15}$$

The following can be obtained:

$$\varphi = \frac{V_p}{V} = 1 - \frac{1-\varphi_0}{1+\varepsilon_v}\left(1 - \frac{\alpha}{K_s}(\Delta P_1 + \Delta P_2) + \Delta\varepsilon_s + \alpha_s\Delta T\right) \tag{16}$$

A dynamic model of coal seam permeability can be derived by using the cubic theorem between permeability and porosity [43]:

$$k = k_0\left(\frac{1}{\varphi_0} - \frac{1-\varphi_0}{\varphi_0(1+\varepsilon_v)}\left(1 - \frac{\alpha}{K_s}(\Delta P_1 + \Delta P_2) + \Delta\varepsilon_s + \alpha_s\Delta T\right)\right)^3 \tag{17}$$

2.6. Physical Parameters

The relevant thermal physical parameters change with temperature and pressure. This study is based on shallow low-rank coal with a buried depth of 450 m, which is relatively shallow. Therefore, the temperature range is 280–310 K and the pressure is 0–10 MPa. Refprop software has been used for physical parameters evaluation (Figures 1 and 2). It can be seen that all the thermal physical parameters change nonlinearly with temperature and pressure. Among them, the physical parameters of CO_2 show a sudden change trend under certain temperatures and pressure. Therefore, it is very unreasonable to regard the thermal physical parameters as constants as previous studies. This paper uses Matlab to call Refprop software, then uses polynomial function fitting in Matlab. It is worth mentioning that the Refprop software is based on the most accurate pure fluid and mixture

models at present. It implements three models for the thermodynamic properties of pure fluids: equations of state explicit in Helmholtz energy, the modified Benedict-Webb-Rubin equation of state, and an extended corresponding states (ECS) model [44]. For CO_2 and CH_4, high accuracy Helmholtz energy equations of state is used.

The relationship between density, specific heat capacity, thermal conductivity, dynamic viscosity and pressure/temperature is fitted as follows. These equations are used for numerical solutions.

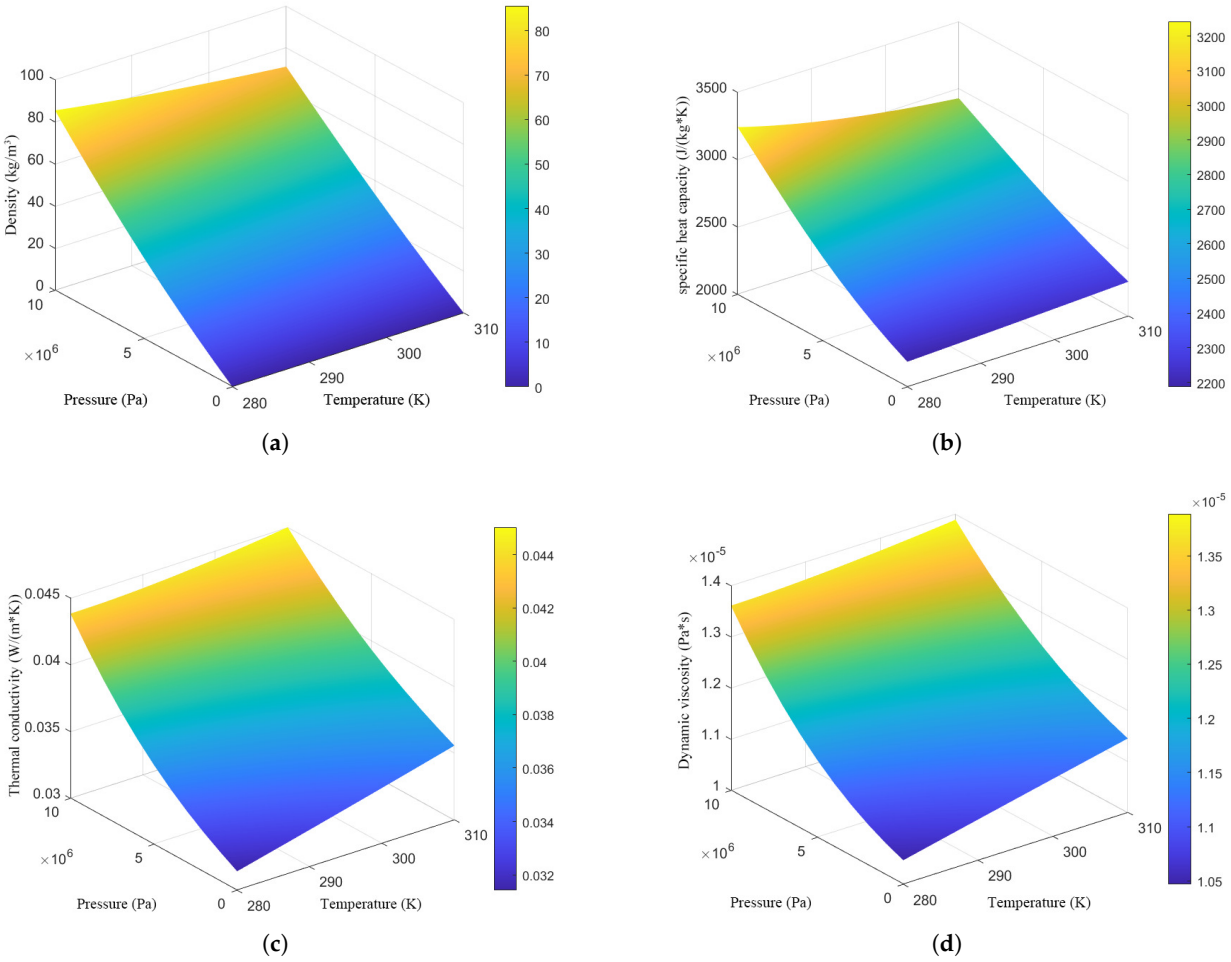


Figure 1. CH_4 (**a**) density, (**b**) specific heat capacity, (**c**) thermal conductivity and (**d**) dynamic viscosity as a function of pressure/temperature.

For CH_4: $T \in [280, 310]$ °C $\quad P \in [0, 10]$ MPa

$$\rho_1 = p00 + p10 \times P_1 + p01 \times T + p20 \times P_1^2 + p11 \times P_1 \times T + p30 \times {P_1}^3 + p21 \times P_1^2 \times T \tag{18}$$

$$C_{g1} = p00 + p10 \times P_1 + p01 \times T + p20 \times P_1^2 + p11 \times P_1 \times T + p30 \times {P_1}^2 + p21 \times P_1^2 \times T \tag{19}$$

$$\lambda_{g1} = p00 + p10 \times P_1 + p01 \times T + p20 \times P_1^2 + p11 \times P_1 \times T + p30 \times P_1^3 + p21 \times P_1^2 \times T \tag{20}$$

$$\mu_1 = p00 + p10 \times P_1 + p01 \times T + p20 \times P_1^2 + p11 \times T \times P_1 \tag{21}$$

For CO_2: $T \in [280, 310]$ °C $\quad P \in [0, 10]$ MPa

$$\rho_2 = p00 + p10 \times P_2 + p20 \times T + p20 \times P_2 \times T \quad (22)$$

$$C_{g2} = p00 + p10 \times P_2 + p01 \times T + p20 \times {P_2}^2 + p11 \times P_2 \times T + p30 \times {P_2}^3 + p21 \times {P_2}^2 \times T \quad (23)$$

$$\lambda_{g2} = p00 + p10 \times P_2 + p01 \times T + p20 \times {P_2}^2 + p11 \times P_2 \times T + p30 \times {P_2}^3 + p21 \times {P_2}^2 \times T \quad (24)$$

$$\mu_2 = p00 + p10 \times P_2 + p01 \times T + p20 \times {P_2}^2 + p11 \times T \times P_2 + p30 \times {P_2}^3 + p21 \times {P_2}^2 \times T \quad (25)$$

where, T is temperature, K; P_i is pressure, Pa; μ_i is the dynamic viscosity, Pa·s; C_{gi} is the specific heat capacity, J/(kg·K); ρ_i is the density, kg/m^3; λ_{gi} is the thermal conductivity, W/(m·K); i = 1, CH_4, i = 2, CO_2. Tables 2 and 3 list the corresponding coefficients in the equation.

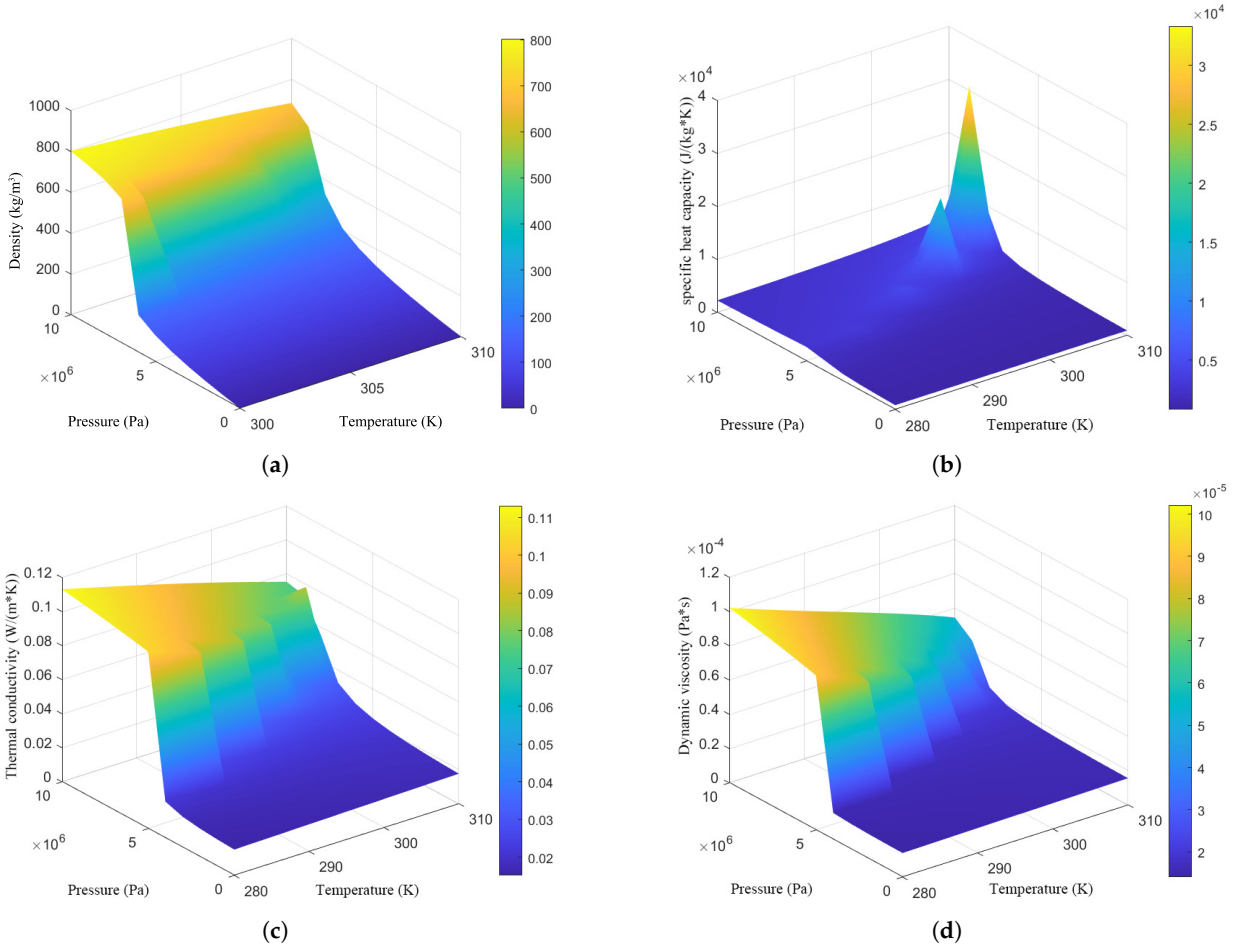


Figure 2. CO_2 (**a**) density, (**b**) specific heat capacity, (**c**) thermal conductivity and (**d**) dynamic viscosity as a function of pressure/temperature.

Table 2. The correlation coefficient of the fitted equation for CH_4.

CH_4	ρ_1	C_{g1}	λ_{g1}	μ_1
$p00$	−12.08	1547	−0.006677	1.501×10^{-06}
$p10$	2.06×10^{-05}	0.0002031	6.235×10^{-10}	-1.858×10^{-14}
$p01$	0.0408	2.282	0.0001361	3.206×10^{-08}
$p20$	1.205×10^{-13}	2.65×10^{-11}	3.108×10^{-16}	9.262×10^{-20}
$p11$	-4.75×10^{-08}	-4.981×10^{-07}	4.881×10^{-14}	4.895×10^{-16}
$p30$	-	-1.045×10^{-19}	1.269×10^{-24}	2.735×10^{-28}
$p21$	-	-7.677×10^{-14}	-9.47×10^{-19}	-2.724×10^{-22}
$R2$	0.9999	0.9995	0.9999	0.9999

Table 3. The correlation coefficient of the fitted equation for CO_2.

CO_2	ρ_2	C_{g2}	λ_{g2}	μ_2
$p00$	-1026	781.6	-0.00621	5.872×10^{-07}
$p10$	0.0002926	-0.0009226	-4.58×10^{-09}	-6.52×10^{-13}
$p01$	8.73	0.1969	7.646×10^{-05}	4.808×10^{-08}
$p20$	5.988×10^{-12}	6.334×10^{-10}	2.761×10^{-15}	4.66×10^{-19}
$p11$	-1.027×10^{-06}	3.455×10^{-06}	1.745×10^{-11}	2.529×10^{-15}
$p30$	-	9.827×10^{-18}	5.218×10^{-23}	1.044×10^{-26}
$p21$	-	-2.217×10^{-12}	-9.643×10^{-18}	-1.573×10^{-21}
$R2$	0.9993	0.9867	0.8925	0.9994

2.7. Cross Coupling of the Thermal-Hydraulic-Mechanical Fields

Cross coupling among CO_2-ECBM is expressed as:

$$\begin{cases} \dfrac{\partial \frac{\varphi}{RT} P_i M_i + \rho_c \rho_i \frac{a_i b_i P_i}{1+b_1 P_1 + b_2 P_2}}{\partial t} - \nabla \cdot \left(\dfrac{k}{\mu_i} \nabla P_i \cdot \rho_i \right) - \dfrac{\varphi}{RT} \nabla \cdot (D_i \nabla P_i) = Q_i \\ G u_{i,j} + \dfrac{G}{1-2v} u_{j,ji} - \alpha P_{1,i} - \alpha P_{2,i} - K \varepsilon_{s,i} + F_i = 0 \\ \dfrac{\partial}{\partial t} \left((\rho C_p)_{eff} \right) + \eta_{eff} \nabla T - \nabla \cdot \left(\lambda_{eff} \nabla T \right) + K \alpha_T T \dfrac{\partial \varepsilon_s}{\partial t} + \sum_{i=1}^{2} q_{sti} \dfrac{\rho_s \rho_{si}}{M_i} \dfrac{\partial \varepsilon_v}{\partial t} = 0 \\ k = k_0 \left(\dfrac{1}{\varphi_0} - \dfrac{1-\varphi_0}{\varphi_0 (1+\varepsilon_v)} \left(1 - - \dfrac{\alpha}{K_s} (\Delta P_1 + \Delta P_2) + \Delta \varepsilon_s \right) \right)^3 \end{cases} \tag{26}$$

Cross coupling among CBM is expressed as:

$$\begin{cases} \dfrac{\partial \frac{\varphi}{RT} P_1 M_1 + \rho_c \rho_1 \frac{a_1 b_1 P_1}{1+b_1 P_1}}{\partial t} - \nabla \cdot \left(\dfrac{k}{\mu_1} \nabla P_1 \cdot \rho_1 \right) - \dfrac{\varphi}{RT} \nabla \cdot (D_i \nabla P_1) = Q_1 \\ G u_{i,jj} + \dfrac{G}{1-2v} u_{j,ji} - \alpha P_{1,i} - K \varepsilon_{s,i} + F_i = 0 \\ \dfrac{\partial}{\partial t} \left((\rho C_p)_{eff} \right) + \eta_{eff} \nabla T - \nabla \cdot \left(\lambda_{eff} \nabla T \right) + K \alpha_T T \dfrac{\partial \varepsilon_s}{\partial t} + \sum_{i=1}^{2} q_{st1} \dfrac{\rho_s \rho_{s1}}{M_1} \dfrac{\partial \varepsilon_v}{\partial t} = 0 \\ k = k_0 \left(\dfrac{1}{\varphi_0} - \dfrac{1-\varphi_0}{\varphi_0 (1+\varepsilon_v)} \left(1 - - \dfrac{\alpha}{K_s} (\Delta P_1 + \Delta P_2) + \Delta \varepsilon_s \right) \right)^3 \end{cases} \tag{27}$$

In summary, a fully coupled temperature-seepage-diffusion-deformation model for CO_2-ECBM and CBM considering the variation of physical parameters is established in Figure 3. The thermal stress caused by the change of coal seam temperature affects the stress field of the coal seam skeleton. The heat generated by the energy dissipation in the coal seam skeleton has an impact on the coal seam temperature; The temperature change causes the gas pressure change to affect the gas; the thermal convection between the gas and coal seam skeleton affects the temperature of the coal seam. The porosity change caused by coal seam deformation affects gas flow. Gas pressure change causes coal seam deformation.

In this study, based on COMSOL Multiphysics software, the established mathematical model is solved by full physical field coupling of the finite element method.

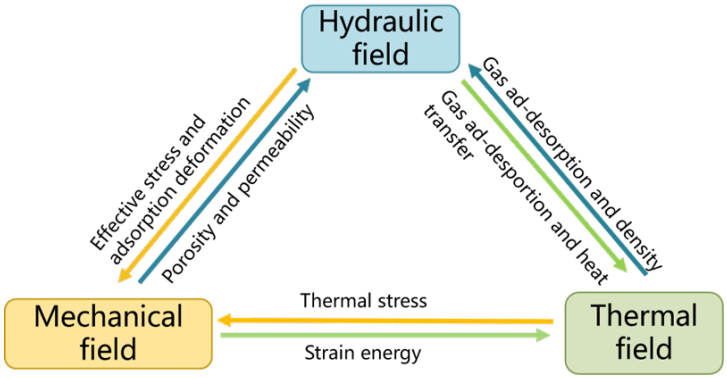


Figure 3. *T-H-M* coupling relationship.

2.8. Model Validation

The Canadian CSEMP project [45] is a rare approach CO_2-ECBM micro-test project for shallow low-rank coal that has undergone multiple productions and multi-component injection processes. The test site is located near Buck Lake in Alder Plain, Canada. The test site consists of Wells 12-28, Well 7-28 and Enerplus Pembina 102/7-28-46-7 W5M (Well Injector). In this paper, based on the two-year initial production of well 12-28, a three-dimensional model is established to simulate the 100*100 m area around well 12-28. The verification model is shown below Figure 4:

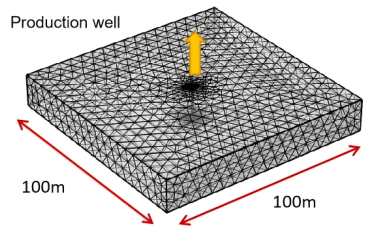


Figure 4. Verify Model Meshing Diagram.

Using the bottom hole pressure to fit the gas injection rate, the following results are obtained in Figure 5. Due to the expansion effect caused by the adsorption and desorption of CO_2 and CH_4, the permeability gradually decreases, as well as the gas rate of injected CO_2. The numerical simulation results are basically consistent with the measured data, and acceptable deviations are determined by the simplification of reservoir's initial anisotropy, and the ignore of CO_2 phase transition. However, the numerical simulation results and field data have the same trend, which can preliminarily illustrate the reliability of the numerical model.

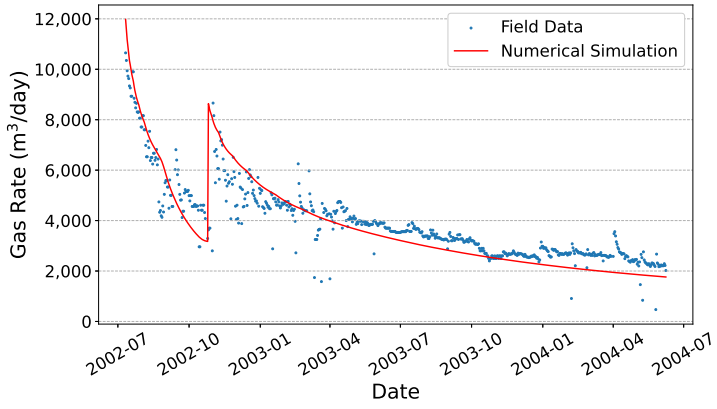


Figure 5. History match of CH_4 production rate during primary CBM recovery.

3. Simulation Scheme

3.1. Simulation Program

We set up three simulation programs. Firstly, this study will compare CBM (directly mining) with CO2-ECBM, in order to affirm the advantages of CO2-ECBM. The evolution of reservoir pressure, permeability and adsorbed gas content in CO2-ECBM and CBM engineering will be analyzed. Subsequently, the effects of different injection pressures and temperatures on CO2-ECBM will be analyzed (Table 4).

Table 4. Simulation program.

Plan	Model	Coupled Mode	Question
A	*CBM* CO_2-*ECBM*	H-M coupling H-M coupling	Effect of CO_2 Injection on *CBM* Exploitation
B	injection pressure: 2 MPa injection pressure: 4 MPa injection pressure: 6 MPa	T-H-M coupling	Effect of CO_2 Injection Pressure on CO_2-*ECBM*
C	injection temperature: 289 K injection temperature: 300 K injection temperature: 320 K	T-H-M coupling	The effect of injection well temperature on CO_2-*ECBM*

3.2. Basic Model

The traditional five-point well pattern layout is used as the research object, and a quarter of the extraction area near the bottom of the well is selected as the simulation area (Figure 6). The actual size is 100 × 100 m. A two-dimensional intercept line is set on the diagonal of the model, and observation points B and C are set near the injection well and the production well. The coordinates of point B and point C are (20 m, 20 m) and (80 m, 80 m) respectively. The initial formation pressure of the coal seam is 1.6 MPa, and the temperature of the coal seam is 289 K. The gas injection boundary condition is constant pressure boundary condition. The production well is connected to the surface, and the bottom hole flowing pressure is 0.1 MPa. Table 5 illustrates the numerical simulation core parameters.

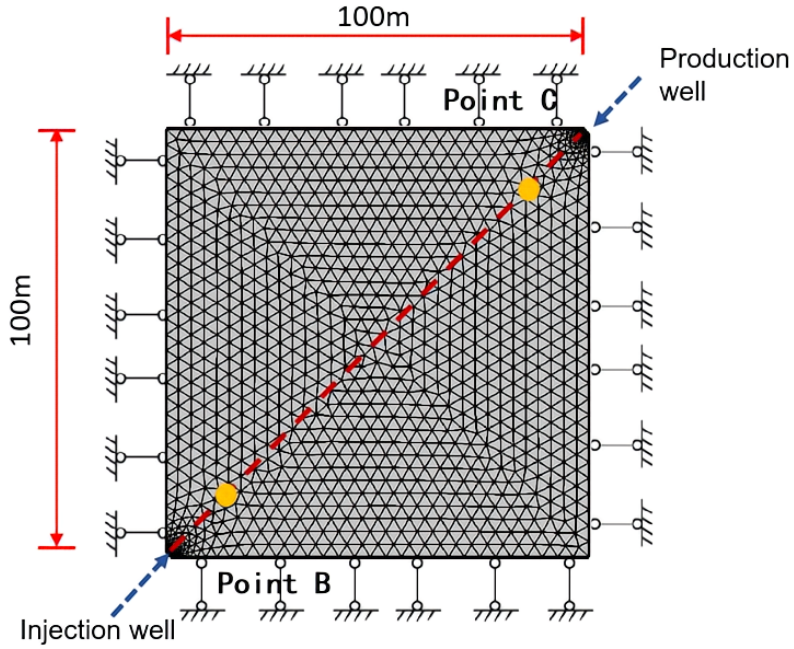


Figure 6. Numerical simulation model for CO_2-*ECBM*.

Table 5. Numerical simulation core parameters (refer to CSEMP project).

Parameter (Unit)	Value	Parameter (Unit)	Value
Thermal expansion coefficienta (K^{-1})	2.4×10^{-5}	Langmuir volumetric strain constant of CH_4 (-)	0.0128
Universal gas constant (J/(K·mol))	8.314	Langmuir volumetric strain constant of CO_2 (-)	0.0237
Initial porosity (-)	0.08	Langmuir pressure of CH_4 (MPa)	3.82
Initial permeability of coalbed (mD)	0.5	Langmuir pressure of CO_2 (MPa)	2.35
Density of coal (kg/m^3)	1785	Langmuir volume constant of CH_4 (m^3/kg)	0.01237
Coalbed temperature (K)	(289)	Langmuir volume constant of CO_2 (m^3/kg)	0.04607
Specific heat capacity of coal (J/(K·kg))	1255	Hydrodynamic dispersion coefficient of CH_4 (m^2/s)	3.6×10^{-11}
Initial coalbed pressure (MPa)	1.6	Hydrodynamic dispersion coefficient of CO_2 (m^2/s)	5.8×10^{-11}
Thermal conductivity of coal (W/(m·K))	0.12	Bulk modulus of coal (MPa)	2500
Poisson's ratio	0.25	Bulk modulus of coal skeleton (MPa)	8134

4. Results and Discussions

4.1. Effect of CO_2 Injection on Coalbed Methane Production

4.1.1. Variation of Reservoir Pressure

Figure 7 shows the distribution of reservoir pressure. During the CBM process, the reservoir pressure gradually decreases with time (Figure 7a). Affected by the pressure relief of the production well, the reservoir pressure begins to decrease from the production well and gradually diffuses into the reservoir. During the CO_2-ECBM process (Figure 7b), reservoir pressure gradually increases with time. At the same production time, CO_2 injection has an enhancement effect on reservoir pressure. When CO_2 is injected, the reservoir pressure near the bottom of the well is greater. As the distance from the well increases, the pressure decreases in a step-wise manner, which indicates that CO_2 mainly accumulates at the bottom of the well and near the well.

According to the Langmuir adsorption theory, the pressure gradient in the reservoir will directly affect the adsorption and desorption of gas in the reservoir (Equation (5)). During the CO_2 injection process, a large amount of CO_2 is adsorbed in the near-well reservoir, which will lead to the rapid decrease of reservoir permeability around the bottom of the well. Finally, it will limit the flow capacity of CO_2 and cause a decrease in injection capacity.

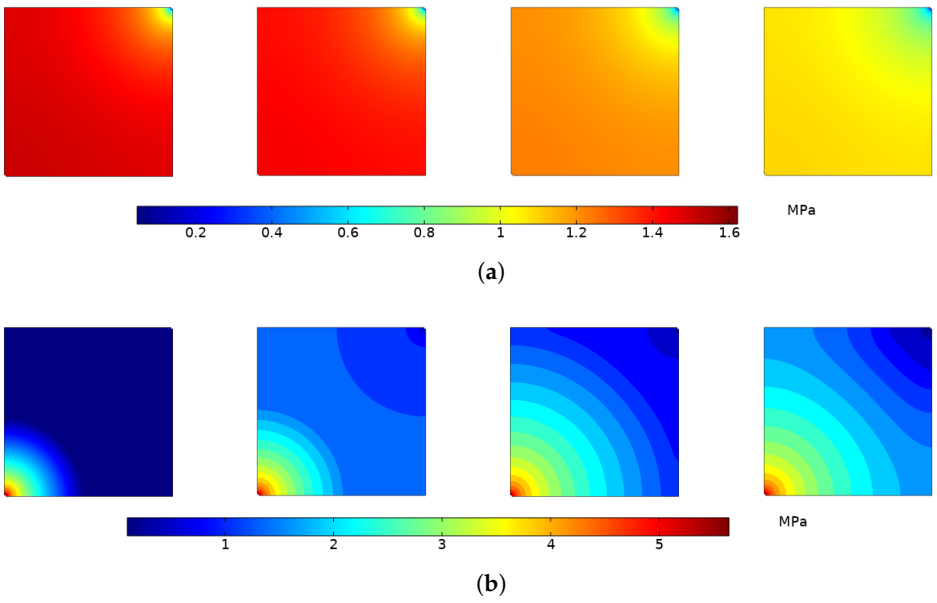


Figure 7. 300 days, 500 days, 1000 days, 1500 days reservoir pressure distribution cloud (**a**) *CBM* (**b**) *CO_2-ECBM*.

Figure 8 presents the distribution of gas pressure along the diagonal. After 1500 days of production, the gas pressure near the injection well is reduced to 1.06 MPa (Figure 8a). Taking the initial gas pressure as a reference, when the production is 300 days, 500 days, 1000 days, 1500 days, the gas pressure near the injection well is 87%, 81%, 75%, 66% of the initial pressure, respectively. During the CO_2-ECBM process, the gas pressure gradually decreases from the injection well to the middle of the reservoir and then to the production well, and the gas pressure increases with time (Figure 8b). The pressure differential between the production well and the injection well is greatly increased compared with the direct exploitation. It is because of a higher pressure differential, gas will accelerate its migration to the production well.

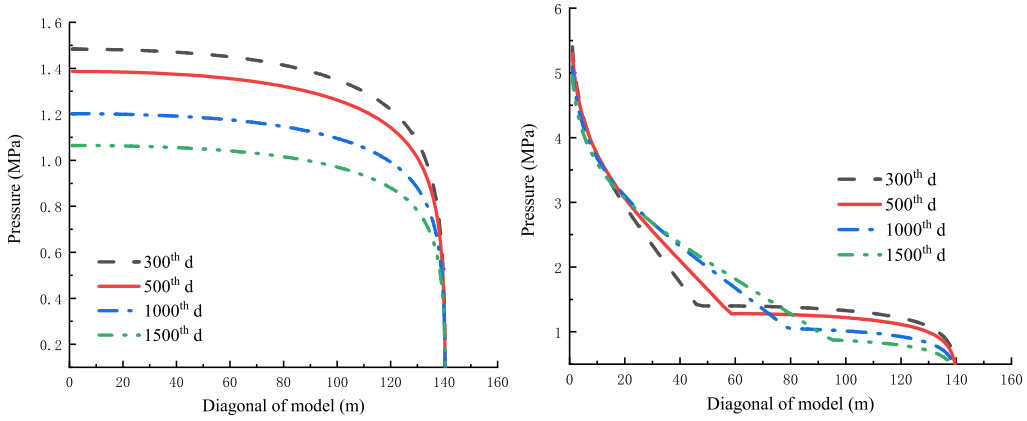


Figure 8. Distribution curve of reservoir gas pressure along the model diagonal (**a**) *CBM* (**b**) *CO_2-ECBM*.

Figure 9 illustrates the distribution of gas pressure at reference point B. The reservoir pressure of point B near the injection well decreases with time. The rate of reservoir pressure reduction is relatively slow at the initial stage because point B is far away from the production well. However, as the influence range of the production radius continues to expand, the reservoir pressure of point B continues to decrease at a higher rate (Figure 9a).

During the CO_2 injection process, after an initial decrease, the reservoir pressure increases rapidly and then the increase rate begins to slow down and even slightly decreases (Figure 9b). The injection of CO_2 first increases the pressure of the reservoir near the injection well. With the progress of CO_2 injection, the pressure increase trend continues to spread to the internal part of the reservoir. After a period of time, it will inevitably affect the reservoir pressure at point B, and increase the pressure at this point. With the injection process, the decrease of the reservoir permeability inhibits the injection rate of CO_2, and the increase of CO_2 pressure will slow down. However, the pressure reduction trend of CH_4 under the influence of the pressure relief of the production well is not be affected. Therefore, the reservoir pressure increases slowly and slightly decreases in the later period.

4.1.2. Variation of CH_4 Concentration

Figure 10 illustrates the distribution of CH_4 concentration. During the direct exploitation (Figure 10a), the CH_4 concentration first changes in the area near the production well and continues to extend into the reservoir. The CH_4 in the reservoir will continuously migrate to the production well because of the pressure differential. However, the pressure differential between the reservoir and the production well is relatively small, the gas migration speed is slow, and the CH_4 concentration changes gradually.

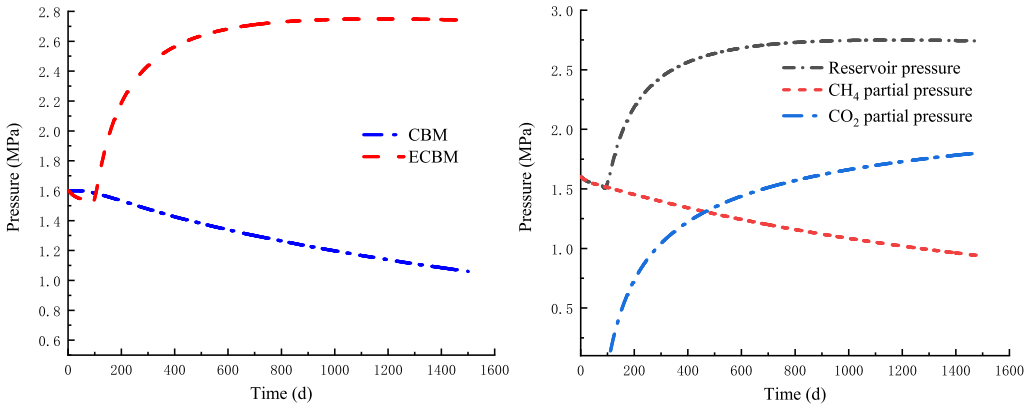


Figure 9. Variation curve of reservoir pressure at reference point B. (**a**) Comparison of *CO_2-ECBM* and CBM (**b**) *CO_2*, *CH_4* partial pressure and total reservoir pressure of *CO_2-ECBM*.

During CO_2 injection mining (Figure 10b), due to the injection of CO_2, the pressure differential from the injection well to the coal seam, to the production well is higher than that of the direct exploitation. Therefore, at the same time, the change in CH_4 concentration alone with CO_2 injection exploitation is higher than that of direct exploitation. Near the injection well, preferential adsorption of CO_2 to the coal seam after injection forces the desorption of adsorbed CH_4. The desorbed CH_4 migrates to the production well under the effect of pressure differential, thus the CH_4 concentration near the injection well is also reduced.

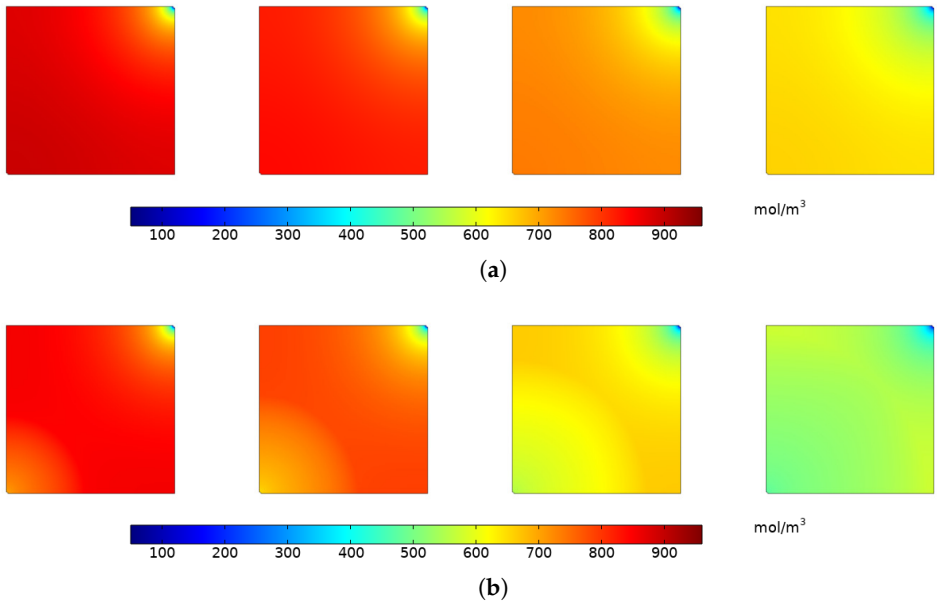


Figure 10. 300 days, 500 days, 1000 days, 1500 days CH_4 content distribution cloud (**a**) *CBM* (**b**) *CO_2-ECBM*.

4.1.3. Variation of Adsorbed Gas Concentration

The core of the CO_2-ECBM is to achieve the purpose of stable CO_2 storage through the adsorption of CO_2 by coal matrix. The adsorption competition between CO_2 and CH_4 is one of the core problems in the process of CO_2 storage in the coal seam. Especially in the injection stage, with the injection of CO_2, the bottom hole and near-well reservoir contain a large pressure range. According to the Langmuir adsorption theory, different pressures determine the adsorption capacity of different gases in the coal seam (Equation (5)).

Figure 11 illustrates the distribution of adsorbed CH_4 concentration in direct exploitation and CO_2 injection exploitation, as well as adsorbed CO_2 concentration in CO_2 injection exploitation. During direct exploitation, the adsorbed CH_4 concentration mainly changes near the production well, but the change is small. Affected by the pressure relief of the production well, the free CH_4 is first extracted, then the dynamic equilibrium of the gas in the pore is broken, and part of the adsorbed CH_4 is desorbed Figure 11a. However, the desorption of adsorbed CH_4 is not high during direct exploitation. When CO_2 is injected into the coal seam, it will preferentially adsorb in the coal matrix because the adsorption of CO_2 is greater than that of CH_4, forcing the latter to desorb. It can be obtained from Figure 11b, With the continuous injection of CO_2, the concentration of adsorbed CH_4 at the injection well and production well continues to decrease. It can also be seen from Figure 11c that as CO_2 is injected, the concentration of adsorbed CO_2 in the reservoir increased dramatically.

In brief, CH_4 desorption is slow and the amount of desorption is small during direct exploitation, which often leads to a small recovery rate of CH_4. The CO_2-ECBM technology has the dual benefits of greenhouse gas emission reduction and clean fossil energy development, and it's superiority to conventional exploration technologies.

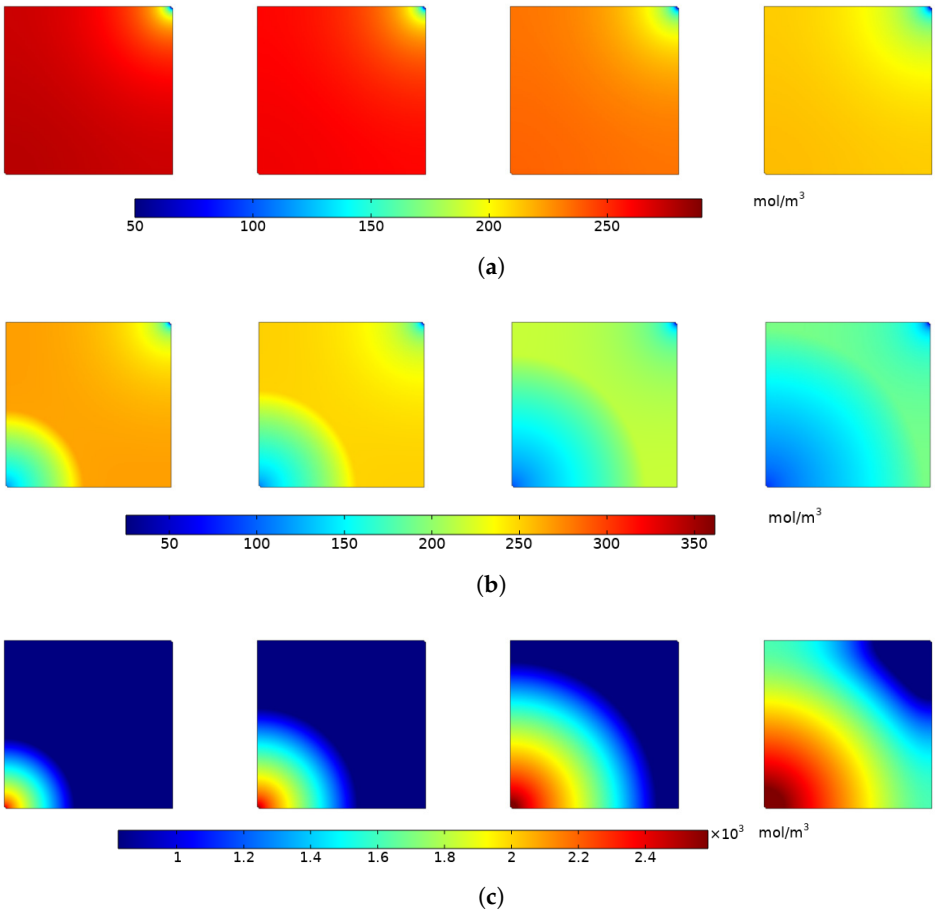


Figure 11. 300 days, 500 days, 1000 days, 1500 days (**a**) Distribution cloud diagram of adsorbed CH_4 in *CBM* (**b**) adsorption cloud diagram of adsorbed CH_4 in CO_2-*ECBM* (**c**) adsorption cloud diagram of adsorbed CO_2 in CO_2-*ECBM*.

4.1.4. Variation of Reservoir Permeability

The scientific connotation of the effectiveness of CO_2-ECBM mainly includes the CO_2 storage mechanism and storage capacity, and the increase rate of CH_4 yield, which are also the basic theoretical and technical problems faced by CO_2-ECBM. The effectiveness

of CO_2-ECBM also becomes the premise and foundation of the safety and economy of CO_2-ECBM. The injectivity of CO_2 can be characterized by injection pressure, injection rate, cumulative injection volume and other parameters, which are mainly related to the permeability of the coal seam and its dynamic changes. Therefore, it is necessary to study the permeability evolution of the reservoir. With the injection of CO_2, the permeability of coal seams will decrease, which often affects the injectivity of CO_2 [46].

The evolution of permeability in the CO_2-ECBM process is a very complex phenomenon, which is determined by the stress effect and the adsorption swelling effect. On the one hand, effective stress increases and permeability decreases because of cleat compression [47]. On the other hand, the matrix expands, the seepage channel is compressed, and the permeability will decrease, along with CO2 adsorption, as CH_4 desorption occurs, matrix shrinkage, seepage channel opens, permeability will increase [46].

During direct exploitation (Figure 12a), the reservoir permeability increases with time, and the closer to the production well is, the higher the permeability will be. This is because with the production, the pressure near the production well decreases, CH_4 desorbs, the matrix shrinks, then the permeability increases. In addition, the increase of effective stress leads to the decrease of permeability. However, the increase of permeability caused by matrix shrinkage deformation dominates. Therefore, the permeability increases compared with the initial permeability.

In the case of CO_2 injection (Figure 12b), for the area near injection well, the decrease of effective stress will lead to the increase of permeability near the gas injection well, while the matrix expansion caused by competitive adsorption will lead to the decrease of permeability. At this time, the expansion deformation caused by the competitive adsorption of CO_2 and CH_4 dominates, and the permeability near the gas injection well decreases rapidly.

For the area near the production well, when the production time is short, the injected CO_2 does not affect the production well. At this time, the stress effect reduces the permeability, and the matrix shrinkage effect caused by CH_4 desorption leads to the increase of permeability, but the matrix shrinkage effect caused by CH_4 desorption dominates. Therefore, the permeability of the production well is larger than the initial permeability.

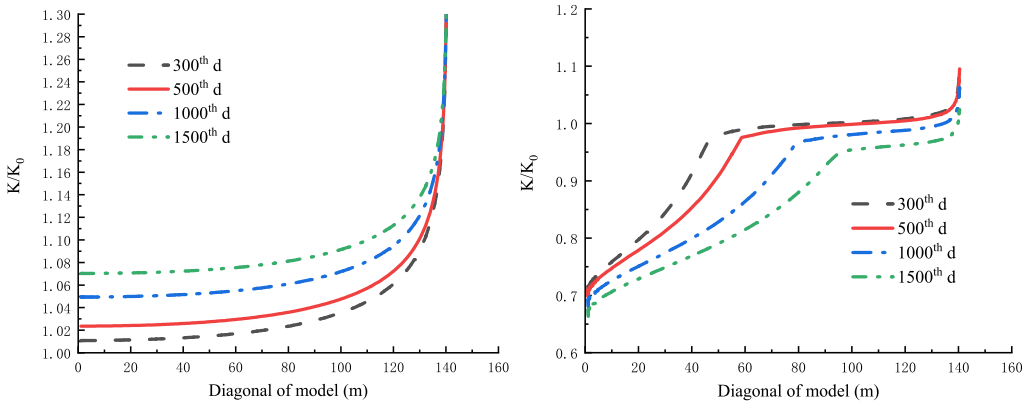


Figure 12. Distribution curve of reservoir permeability along the model diagonal (**a**) *CBM* (**b**) *CO_2-ECBM*.

4.2. Effect of Different Injection Pressure on CO_2-ECBM

4.2.1. Variation of Reservoir Pressure

In the process of CO_2-ECBM, the gas pressure continues to increase with time, and with the increase of injection pressure, the gas pressure in the reservoir changes more obviously (Figure 13). Especially in the early stage of gas injection, increasing the injection pressure can make the gas pressure in the reservoir increase rapidly in a short time, making CH_4 gas easier to produce. The pressure differential and concentration differential are the driving force of the seepage and diffusion of CO_2 and CH_4 in the coal seam. When CO_2

is injected, the reservoir pressure is greatly increased, and the pressure differential is also increased, which promotes the gas to flow and diffuse to the production well faster. This is one of the reasons why CO_2 injection can increase the production of coalbed methane.

4.2.2. Optimal Injection Pressure Selection

Figure 14a,b illustrate the distribution of cumulative production and point B's permeability change during CO_2 injection exploitation under the pressure of 1 MPa to 6 MPa. The permeability near the injection well is lower than the initial permeability, and the permeability decreases with the increase of injection pressure at the same production time. This is because the increase of gas injection pressure will lead to the increase of reservoir adsorption amount, which will lead to the decrease of permeability. The decrease of permeability will limit the flow capacity of CO_2 and weaken the injection capacity. In this study, point B near the injection well is taken to analyze the change of reservoir permeability near the well when the injection pressure changes. It can be seen that when the injection pressure increases, the permeability of a point near the injection well decreases rapidly. When the injection pressure is 6 MPa, the reservoir permeability decreases by 0.6 times of the initial permeability. At the same time, as the injection pressure increases, the pressure differential in the reservoir increases, prompting faster gas seepage and diffusion, and CH_4 production will increase. When the injection pressure is 6 MPa, the CH_4 production increases to 3.79×10^5 m^3, which is 75% higher than that when the injection pressure is 1 MPa.

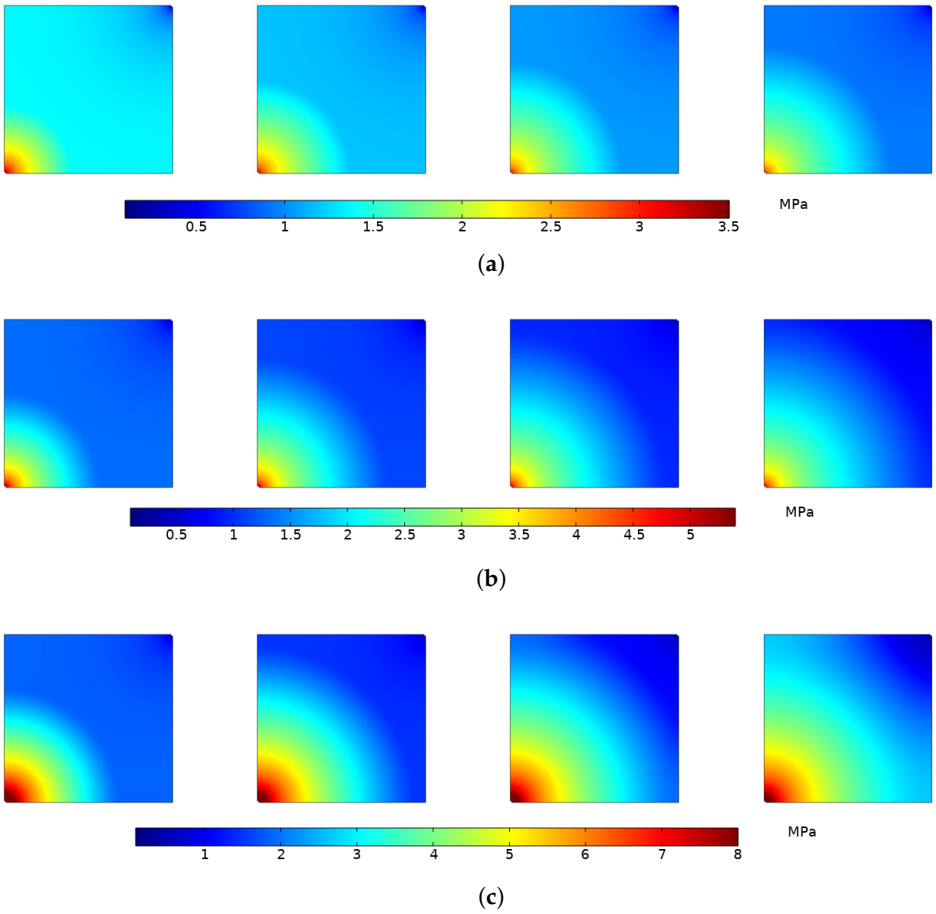
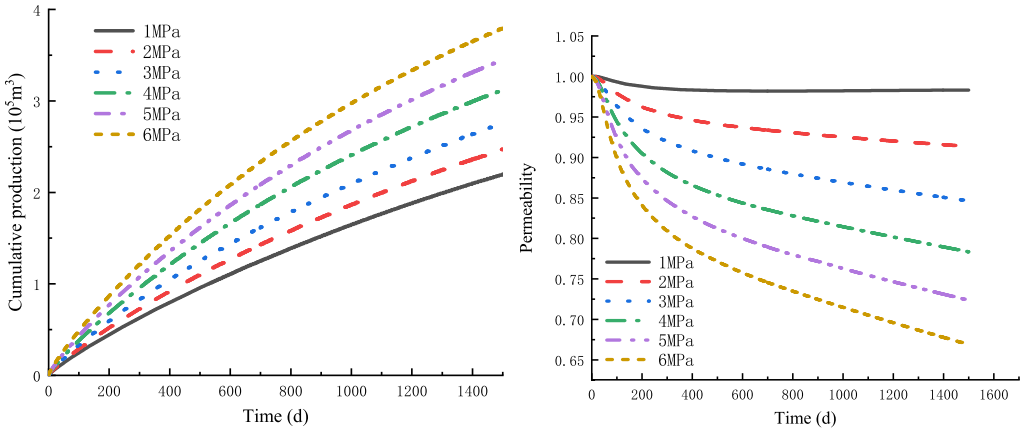


Figure 13. 300 days, 500 days, 1000 days, 1500 days Reservoir pressure cloud diagram (**a**) The injection pressure is 2 MPa (**b**) The injection pressure is 4 MPa (**c**) The injection pressure is 6 MPa.

In summary, increasing gas injection pressure can promote CH_4 production and CO_2 storage, but the increase of gas injection pressure will also lead to rapid attenuation of

near-well reservoir permeability, resulting in the weakening of injection capacity. We analyzed the change rate of CH_4 production. The peak value of the change rate of CH_4 production was 0.153 at 3 MPa, indicating that the injection pressure continued to increase after the displacement pressure reached 3 MPa, and the recovery degree did not change much. Consequently, we can take 3 MPa as the optimal injection pressure in this case.



(**a**) (**b**)

Figure 14. (**a**): Cumulative production. (**b**): Permeability change at point B.

4.3. Effect of Different Injection Temperatures on CO_2-ECBM

4.3.1. Variation of Reservoir Temperature

Figure 15 illustrates the reservoir temperature distribution. When the injection temperature is the same as the reservoir temperature, the temperature increases near the injection well due to the adsorption of CO_2, and the temperature near the production well decreases due to CH_4 desorption. After the gas injection, CO_2 adsorption induced an exothermic effect and the reservoir temperature near the injection well rose sharply [48]. Meanwhile, the range affected by temperature gradually increased due to heat conduction. CH_4 desorption promoted a reduction in reservoir temperature near the production well.

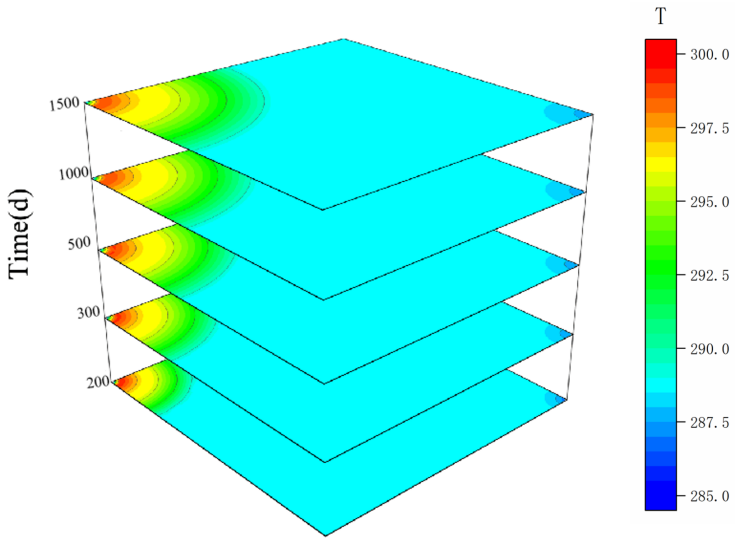


Figure 15. Reservoir temperature distribution.

In addition to the thermodynamic effect of Hydraulic-Mechanical interaction and the temperature effect of non-isothermal adsorption, the internal energy change in the reservoir also has the Thermal-Hydraulic coupling of the fluid itself caused by the change of CO_2 phase state, that is, the phenomenon of liquefaction exothermic and gasification

endothermic [49]. In thermochemistry, it is the energy absorbed or released by a substance during a change of state (phase change) without a change in temperature that we call the latent heat of phase change. The heat which is required to melt a certain quantity of a solid at the melting point into a liquid at the same temperature is called the latent heat of fusion. The conversion of the liquid into vapour requires an amount of 'latent heat' which is generally much greater than the latent heat of fusion of the same substance [50]. In the process of CO_2 vaporization, the distance between molecules increases, the molecular force does negative work, and the molecular potential energy increases; where the molecular potential energy is the energy that molecules have with respect to their relative positions due to the mutual forces that exist between them. This process may release or absorb large amounts of heat, but this phenomenon has not been considered in this and previous studies.

4.3.2. Effect of Temperature on CH_4 Production and CO_2 Storage

Figures 16 and 17 illustrate the CH_4 cumulative production and CO_2 cumulative storage of three different temperatures. It is clear that increasing the injection temperature will reduce CH_4 production and CO_2 sequestration. Based on the adsorption potential theory, the increase in temperature has a negative impact on the adsorption of CO_2 and CH_4 in the coal seam, that is, the lower the temperature, the higher the amount of CO_2 and CH_4 adsorbed by coal [9]. Meanwhile, with the increase in temperature, the main reason for the decrease in the ability of CO_2 to replace CH_4 is that the change rate of CO_2 potential energy and diffusion capacity is more significant than that of CH_4, resulting in the decrease of the amount of CO_2 adsorbed by coal seam [10].

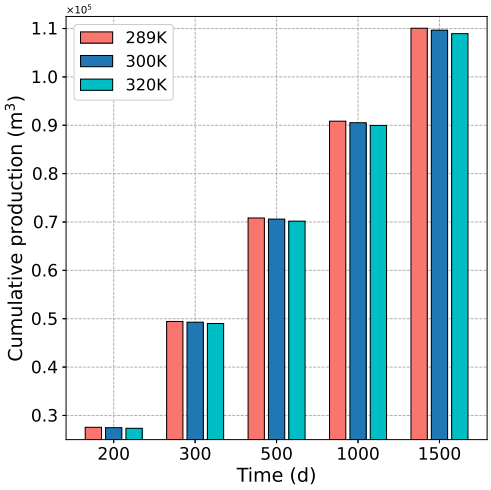


Figure 16. Cumulative production comparison.

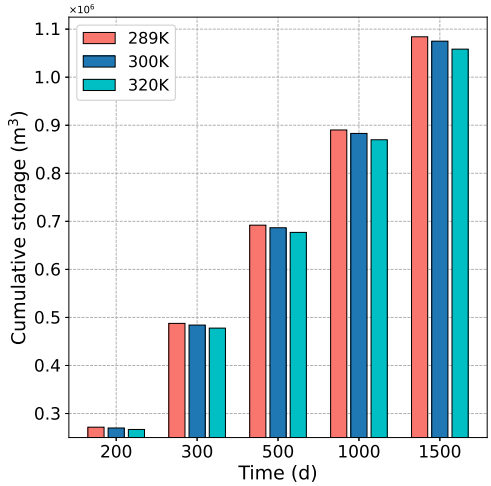


Figure 17. Cumulative CO_2 storage comparison.

5. Conclusions

This paper combines the specific engineering parameters of the CSEMP shallow low-rank coal project and establishes a coupled Thermal-Hydraulic-Mechanical model, which achieves the dynamic evolution of fluid physical parameters and is of great interest as a new guide for the preliminary design of subsequent CO_2-ECBM projects based on shallow low-rank coal. Based on COMSOL Multi-physics software, the finite element method is used to solve the multi-physical field coupling. The following conclusions are obtained:

1. During direct mining, the reservoir pressure shows a downward trend, and the downward trend gradually slows down and tends to be stable. During CO_2 injection, the reservoir pressure increases with time, increases rapidly at the initial stage and gradually tends to be stable. The injection of CO_2 has a significant enhancement effect on coalbed methane extraction.
2. For direct mining, the increase in permeability caused by matrix shrinkage deformation dominates, and the reservoir permeability gradually increases with time, and the closer to the production well, the greater the permeability. For CO_2 injection, the volumetric strain effect caused by adsorption and desorption is dominant in both production wells and injection wells. The permeability near the injection well decreases rapidly and the permeability near the production well increases.
3. Increasing the gas injection pressure can promote the production of CH_4 and the storage of CO_2, but the increase of gas injection pressure will also lead to the rapid attenuation of near-well reservoir permeability and the weakening of injection capacity. When the gas injection pressure reaches 3MPa, the injection pressure continues to increase, and the recovery degree does not change much.
4. When the injection temperature increases, the CO_2 concentration is relatively reduced, and the replacement effect of CH_4 is weakened, resulting in a slight decrease in CBM production and CO_2 burial stock.

6. Future Work

For future works, the different data that have been yielded by the several adopted approaches can be integrated into a supervised learning process. This artificial intelligence technique has been extensively used to describe geological assets [51–55]. It shows its strength by combining different correlated factors and seek their contribution towards the investigated phenomena.

Author Contributions: Conceptualization, H.L., Q.M., K.J. and F.H.; Formal analysis, H.L. and Q.M.; Funding acquisition, H.L.; Investigation, H.L. and Q.M.; Methodology, H.L. and Q.M.; Software, Q.M.; Supervision, H.L.; Validation, Q.M.; Visualization, Q.M. and F.H.; Writing—original draft, H.L., Q.M. and K.J.; Writing—review & editing, H.L. All authors have read and agreed to the published version of the manuscript.

Funding: This research received no external funding.

Institutional Review Board Statement: Not applicable.

Informed Consent Statement: Not applicable.

Data Availability Statement: Not applicable.

Acknowledgments: This study is supported by Open Research Fund of State Key Laboratory of Geomechanics and Geotechnical Engineering, Institute of Rock and Soil Mechanics, Chinese Academy of Sciences, Grant NO. SKLGME021021. The authors thank the support from Ministry of Science and Technology of China through High-end Foreign Specialist Introduction Program with project Grant NO. G2021127005L. The authors thank the support from Fundamental Research Funds for the Central Universities with project Grant NO. DUT20GJ204. This study is supported by Key Laboratory of Deep Earth Science and Engineering (Sichuan University), Ministry of Education, Grant NO. DUSEYU202303.

Conflicts of Interest: The authors declare no conflict of interest.

References

1. Yu, G.; Hao, T.; Zhu, J. Discussion on action strategies of China's carbon peak and carbon neutrality. *Bull. Chin. Acad. Sci.* **2022**, *37*, 423–434.
2. Yao, J.; Han, H.; Yang, Y.; Song, Y.; Li, G. A Review of Recent Progress of Carbon Capture, Utilization, and Storage (CCUS) in China. *Appl. Sci.* **2023**, *13*, 1169. [CrossRef]
3. Sarkodie, S.A.; Strezov, V. Effect of foreign direct investments, economic development and energy consumption on greenhouse gas emissions in developing countries. *Sci. Total Environ.* **2019**, *646*, 862–871. [CrossRef]
4. Adedoyin, F.F.; Gumede, M.I.; Bekun, F.V.; Etokakpan, M.U.; Balsalobre-Lorente, D. Modelling coal rent, economic growth and CO_2 emissions: does regulatory quality matter in BRICS economies? *Sci. Total Environ.* **2020**, *710*, 136284. [CrossRef]
5. Xian, Z. The Application Prospect of CCUS in China under the Target of Carbon Neutrality. *China Sustain. Trib.* **2020**, *12*, 22–24.
6. Zhao, X.; Liao, X.; He, L. The evaluation methods for CO_2 storage in coal beds, in China. *J. Energy Inst.* **2016**, *89*, 389–399. [CrossRef]
7. Shu, S.; Liu, L.; Wang, W. *Theory and Evaluation of the Effectiveness of Deep Coalbed CO_2 Geological Storage and Enhanced Coalbed Methane Development*, 1st ed.; Science Press: Beijing, China, 2020.
8. Dutka, B. CO_2 and CH_4 sorption properties of granular coal briquettes under in situ states. *Fuel* **2019**, *247*, 228–236. [CrossRef]
9. Sun, X.; Yao, Y.; Liu, D. The behavior and efficiency of methane displaced by CO_2 in different coals and experimental conditions. *J. Nat. Gas Sci. Eng.* **2021**, *93*, 104032. [CrossRef]
10. Sijian, Z.; Shuxun, S.; Yanbin, Y.; Dameng, L.; Shiqi, L. Characterization of CO_2 adsorption and displacement of methane in coals: An NMR relaxation method. *Coal J.* **2022**, *47*, 3738–3745. [CrossRef]
11. Xu, Y.; Chen, X.; Yu, J. Experimental Study of the Radial Multi-Scale Dynamic Diffusion Model for Gas-Bearing Coal. *Min. Miner. Depos.* **2022**, *16*, 80–86. [CrossRef]
12. Chen, L.; Zhao, M.; Li, X.; Liu, Y. Impact research of CH4 replacement with CO_2 in hydrous coal under high pressure injection. *Min. Miner. Depos.* **2022**, *16*, 121–126. [CrossRef]
13. Michael, G.; Anders, D.E.; Law, B.E. Geochemical Evaluation of Upper Cretaceous Fruitland Formation Coals, San Juan Basin, New Mexico and Colorado. *Org. Geochem.* **1993**, *20*, 475–498. [CrossRef]
14. Morse, D.G.; Mastalerz, M.; Drobniak, A.; Rupp, J.A.; Harpalani, S. Variations in Coal Characteristics and Their Possible Implications for CO_2 Sequestration: Tanquary Injection Site, Southeastern Illinois, USA. *Int. J. Coal Geol.* **2010**, *84*, 25–38. [CrossRef]
15. Eble, C.F.; Greb, S.F. Palynologic, Petrographic and Geochemical Composition of the Vancleve Coal Bed in Its Type Area, Eastern Kentucky Coal Field, Central Appalachian Basin. *Int. J. Coal Geol.* **2016**, *158*, 1–12. [CrossRef]
16. Botnen, L.S.; Fisher, D.W.; Dobroskok, A.A.; Bratton, T.R.; Greaves, K.H.; Robert McLendon, T.; Steiner, G.; Sorensen, J.A.; Steadman, E.N.; Harju, J.A. Field Test of CO_2 Injection and Storage in Lignite Coal Seam in North Dakota. *Energy Procedia* **2009**, *1*, 2013–2019. [CrossRef]
17. Pashin, J.C.; Clark, P.E.; McIntyre-Redden, M.R.; Carroll, R.E.; Esposito, R.A.; Oudinot, A.Y.; Koperna, G.J. SECARB CO_2 Injection Test in Mature Coalbed Methane Reservoirs of the Black Warrior Basin, Blue Creek Field, Alabama. *Int. J. Coal Geol.* **2015**, *144–145*, 71–87. [CrossRef]
18. He, Q.; Mohaghegh, S.D.; Gholami, V. A Field Study on Simulation of CO_2 Injection and ECBM Production and Prediction of CO_2 Storage Capacity in Unmineable Coal Seam. *J. Pet. Eng.* **2013**, *2013*, 1–8. [CrossRef]
19. Gentzis, T.; Goodarzi, F.; Cheung, F.; Laggoun-Défarge, F. Coalbed Methane Producibility from the Mannville Coals in Alberta, Canada: A Comparison of Two Areas. *Int. J. Coal Geol.* **2008**, *74*, 237–249. [CrossRef]
20. Weniger, P.; Franců, J.; Hemza, P.; Krooss, B.M. Investigations on the Methane and Carbon Dioxide Sorption Capacity of Coals from the SW Upper Silesian Coal Basin, Czech Republic. *Int. J. Coal Geol.* **2012**, *93*, 23–39. [CrossRef]
21. Fujioka, M.; Yamaguchi, S.; Nako, M. CO_2-ECBM Field Tests in the Ishikari Coal Basin of Japan. *Int. J. Coal Geol.* **2010**, *82*, 287–298. [CrossRef]
22. Wong, S.; Law, D.; Deng, X.; Robinson, J.; Kadatz, B.; Gunter, W.D.; Jianping, Y.; Sanli, F.; Zhiqiang, F. Enhanced Coalbed Methane and CO_2 Storage in Anthracitic Coals—Micro-pilot Test at South Qinshui, Shanxi, China. *Int. J. Greenh. Gas Control* **2007**, *1*, 215–222. [CrossRef]
23. Jianping, Y.; Zhang, B.; Wong, S. Test of and Evaluation on Elevation of Coalbed Methane Recovery Ratio by Injecting and Burying CO_2 for 3#Coal Seam of North Section of Shizhuang, Qingshui Basin, Shanxi. *Strateg. Study CAE* **2012**, *14*, 38–44.
24. Pan, Z.; Connell, L.; Shangzhi, M.; Sander, R.; Camilleri, M.; Down, D.I.; Carras, J.; Lu, M.; Xiaokang, F.; Wenzhong, Z.; et al. CO_2 Injectivity in a Multi-lateral Horizontal Well in a Low Permeability Coal Seam: Results from a Field Trial. *Energy Procedia* **2013**, *37*, 5834–5841. [CrossRef]
25. Vishal, V.; Singh, L.; Pradhan, S.P.; Singh, T.N.; Ranjith, P. Numerical modeling of Gondwana coal seams in India as coalbed methane reservoirs substituted for carbon dioxide sequestration. *Energy* **2013**, *49*, 384–394. [CrossRef]
26. Siriwardane, H.J.; Bowes, B.D.; Bromhal, G.S.; Gondle, R.K.; Wells, A.W.; Strazisar, B.R. Modeling of CBM production, CO_2 injection, and tracer movement at a field CO_2 sequestration site. *Int. J. Coal Geol.* **2012**, *96*, 120–136. [CrossRef]

27. Wu, Y.; Liu, J.; Elsworth, D.; Chen, Z.; Connell, L.; Pan, Z. Dual Poroelastic Response of a Coal Seam to CO_2 Injection. *Int. J. Greenh. Gas Control* **2010**, *4*, 668–678. [CrossRef]
28. Yongkang, W. Experiment and Numerical Simulation Analysis of Displacing CH_4 by CO_2 Injection. Master's Thesis, China University of Mining & Technology, Beijing, China, 2016.
29. Fang, H.H.; Sang, S.X.; Liu, S.Q. Numerical simulation of enhancing coalbed methane recovery by injecting CO_2 with heat injection. *Pet. Sci.* **2019**, *16*, 32–43. [CrossRef]
30. Fang, H.; Sang, S.; Liu, S. Establishment of dynamic permeability model of coal reservoir and its numerical simulation during the CO_2-ECBM process. *J. Pet. Sci. Eng.* **2019**, *179*, 885–898. [CrossRef]
31. Kumar, H.; Elsworth, D.; Mathews, J.P.; Liu, J.; Pone, D. Effect of CO_2 injection on heterogeneously permeable coalbed reservoirs. *Fuel* **2014**, *135*, 509–521. [CrossRef]
32. Wang, G.; Wang, K.; Jiang, Y.; Wang, S. Reservoir permeability evolution during the process of CO_2-enhanced coalbed methane recovery. *Energies* **2018**, *11*, 2996. [CrossRef]
33. Gang, B.A.I.; Xihua, Z.; Shiping, W.E.I.; Chaojun, F.A.N.; Xueming, L.I. Simulation and Test of Enhancement of Gas Drainage through CO_2 Injection into Coal Seam of Low Permeability. *Coal Geol. Explor.* **2019**, *47*, 77–84.
34. Su, E.; Liang, Y.; Zou, Q.; Xu, M.; Sasmito, A.P. Numerical analysis of permeability rebound and recovery during coalbed methane extraction: Implications for CO_2 injection methods. *Process. Saf. Environ. Prot.* **2021**, *149*, 93–104. [CrossRef]
35. Yudong, H.; Saipeng, H.; Jian, H.; Xingbin, L.; Lianfu, H.; Changfeng, F. Numerical Simulation of the Effect of Injected CO_2 Temperature and Pressure on CO_2-Enhanced Coalbed Methane. *Appl. Sci.* **2020**, *10*, 1385. [CrossRef]
36. Zhang, J.; Huang, Y. Some Suggestions on the Construction of an Integrated Gas Supply Security Index in China. *Nat. Gas Ind.* **2015**, *35*, 125–128. [CrossRef]
37. Chen, Z.; Liu, J.; Elsworth, D.; Connell, L.D.; Pan, Z. Impact of CO_2 Injection and Differential Deformation on CO_2 Injectivity under In-Situ Stress Conditions. *Int. J. Coal Geol.* **2010**, *81*, 97–108. [CrossRef]
38. Yin, G.; Deng, B.; Li, M.; Zhang, D.; Wang, W.; Li, W.; Shang, D. Impact of Injection Pressure on CO_2–Enhanced Coalbed Methane Recovery Considering Mass Transfer between Coal Fracture and Matrix. *Fuel* **2017**, *196*, 288–297. [CrossRef]
39. Yin, G.Z.; Li, M.H.; Li, S.Z.; Li, W.P.; Yao, J.W.; Zhang, Q.G. 3D Numerical Simulation of Gas Drainage from Boreholes Based on Solid Gas Coupling Model of Coal Containing Gas. *J. China Coal Soc.* **2013**, *38*, 535–541.
40. Fan, Y.; Deng, C.; Zhang, X.; Li, F.; Wang, X.; Qiao, L. Numerical Study of CO_2-enhanced Coalbed Methane Recovery. *Int. J. Greenh. Gas Control* **2018**, *76*, 12–23. [CrossRef]
41. Tao, Y.; Xu, J.; Cheng, M.; Li, S.; Peng, S. Theoretical Analysis and Experimental Study on Permeability of Gas-Bearing Coal. *Yanshilixue Yu Gongcheng Xuebao/Chin. J. Rock Mech. Eng.* **2009**, *28*, 3363–3370.
42. Kong, X.; Wang, E.; Liu, Q.; Li, Z.; Li, D.; Cao, Z.; Niu, Y. Dynamic Permeability and Porosity Evolution of Coal Seam Rich in CBM Based on the Flow-Solid Coupling Theory. *J. Nat. Gas Sci. Eng.* **2017**, *40*, 61–71. [CrossRef]
43. Chilingar, G.V. Relationship Between Porosity, Permeability, and Grain-Size Distribution of Sands and Sandstones. In *Developments in Sedimentology*; Deltaic and Shallow Marine Deposits; van Straaten, L.M.J.U., Ed.; Elsevier: Amsterdam, The Netherlands, 1964; Volume 1, pp. 71–75. [CrossRef]
44. Lemmon, E.W.; Huber, M.L.; McLinden, M.O. NIST reference fluid thermodynamic and transport properties–REFPROP. *NIST Stand. Ref. Database* **2002**, *23*, v7.
45. Gou, S.; Li, H.; Li, J.; Zhao, Y. Effective Means to Alleviate the Greenhouse Effect: Case Study of History Match Simulations on a Brief CO_2 Injection into Less-Deep Low-Rank Coal Seams. *Arab. J. Geosci.* **2021**, *14*, 803. [CrossRef]
46. Niu, Q.; Cao, L.; Sang, S.; Zhou, X.; Wang, W.; Yuan, W.; Ji, Z.; Wang, H.; Nie, Y. Study on the anisotropic permeability in different rank coals under influences of supercritical CO_2 adsorption and effective stress and its enlightenment for CO_2 enhance coalbed methane recovery. *Fuel* **2020**, *262*, 116515. [CrossRef]
47. Palmer, I.; Mansoori, J. How permeability depends on stress and pore pressure in coalbeds: A new model. In Proceedings of the SPE Annual Technical Conference and Exhibition, Denver, CO, USA, 6–9 October 1996.
48. Gao, T.; Zhao, D.; Wang, C.; Feng, Z. Energy variation in coal samples with different particle sizes in the process of adsorption and desorption. *J. Pet. Sci. Eng.* **2020**, *188*, 106932. [CrossRef]
49. Perrot, P. *A to Z of Thermodynamics*; Oxford University Press: Oxford, UK, 1994.
50. Maxwell, J.C. *Theory of Heat*; Longmans, Green, and Company: Harlow, UK, 1872.
51. Younes, K.; Grasset, L. Comparison of thermochemolysis and classical chemical degradation and extraction methods for the analysis of carbohydrates, lignin and lipids in a peat bog. *J. Anal. Appl. Pyrolysis* **2018**, *134*, 61–72. [CrossRef]
52. Younes, K.; Grasset, L. Analysis of molecular proxies of a peat core by thermally assisted hydrolysis and methylation-gas chromatography combined with multivariate analysis. *J. Anal. Appl. Pyrolysis* **2017**, *124*, 726–732. [CrossRef]
53. Younes, K.; Laduranty, J.; Descostes, M.; Grasset, L. Molecular biomarkers study of an ombrotrophic peatland impacted by an anthropogenic clay deposit. *Org. Geochem.* **2017**, *105*, 20–32. [CrossRef]

54. Younes, K.; Grasset, L. The application of DFRC method for the analysis of carbohydrates in a peat bog: Validation and comparison with conventional chemical and thermochemical degradation techniques. *Chem. Geol.* **2020**, *545*, 119644. [CrossRef]
55. Younes, K.; Grasset, L. Carbohydrates as proxies in ombrotrophic peatland: DFRC molecular method coupled with PCA. *Chem. Geol.* **2022**, *606*, 120994. [CrossRef]

Disclaimer/Publisher's Note: The statements, opinions and data contained in all publications are solely those of the individual author(s) and contributor(s) and not of MDPI and/or the editor(s). MDPI and/or the editor(s) disclaim responsibility for any injury to people or property resulting from any ideas, methods, instructions or products referred to in the content.